The Evolution of the Intergalactic Medium Transmission to Redshift Six

Antoinette Songaila[1]

Institute for Astronomy, University of Hawaii, 2680 Woodlawn Drive, Honolulu, HI 96822

Received _____; accepted _____

To be published in Astronomical Journal, May 2004

[1]Visiting astronomer, W. M. Keck Observatory, jointly operated by the California Institute of Technology and the University of California.

ABSTRACT

We have measured the transmission of the Lyα forest produced by neutral hydrogen scattering in the intergalactic medium between redshifts 2 and 6.3 using high signal to noise, high resolution ($R \geq 5000$) observations of 50 quasars spread over the redshift range. We use a uniform set of 15 Å intervals covering Lyα, Lyβ, and Lyγ absorption regions to tabulate the forest transmission as a function of redshift. The transmitted fractions show a relatively smooth evolution over the entire range of redshifts, which can be modelled with a smoothly decreasing ionization rate. Previous claims of an abrupt change at $z \sim 6$ appear in part to be a consequence of an incorrect conversion of Lyβ to Lyα optical depths. The tabulated transmissions can be used to calculate the colors of objects with a specified input spectrum as a function of redshift. We calculate the colors of a flat f_ν galaxy with a large intrinsic continuum break, as an important example.

Subject headings: early universe — intergalactic medium — quasars: absorption lines — galaxies: formation

1. Introduction

The epoch of hydrogen reionization is one of the landmarks of the high redshift universe, providing constraints on the first light sources to have formed and a crucial input to models of structure formation. Recent dramatic progress has been made in determining limits on this redshift, leading to an interesting observational situation. On the one hand, spectroscopy of the Lyman α forest shows that the intergalactic medium (IGM) is highly ionized at $z < 6$, becoming progressively opaque to radiation blueward of the quasars' Lyα emission, culminating in the spectrum of the $z = 6.28$ QSO SDSS 1030+0524 which exhibits a substantial dark region that is consistent with no transmitted flux, i.e. a Gunn-Peterson trough at $z = 6.05$ (Becker et al. 2002, Songaila & Cowie 2002; Fan et al. 2002). This high opacity has been used to infer that this redshift is at the tail end of the hydrogen reionization epoch (Becker et al. 2002; Djorgovski et al. 2002) and comparison with simulations suggest the IGM could have been fully neutral at $z = 6.5$ (Cen & McDonald 2002; Gnedin 2002; Fan et al. 2002) though, as we point out in this paper, some of the strongest claims in this regard are based on an incorrect conversion of Lyβ opacities to equivalent Lyα opacities (Becker et al. 2002; White et al. 2003). On the other hand, the recent detection by WMAP of a large optical depth to electron scattering (Bennett et al. 2003) is consistent with the Universe having been reionized at $z \sim 15$ and fully ionized thereafter.

The exact significance of the Gunn-Peterson trough in SDSS 1030+0524 is still not clear. It could follow from the ongoing thickening of the Lyα forest rather than representing the onset of reionization since it is extremely difficult to distinguish the two effects. The discovery of three new $z > 6$ SDSS quasars (Fan et al. 2003) has made the situation more complex since, as might have been expected, there is significant variance in opacity between different lines of sight at $z \sim 6$ (Fan et al. 2003; White et al. 2003). Although White et al. (2003) have argued that apparent increased transmission in the spectrum of SDSS 1148+5251, currently

the highest redshift quasar, could be a result of foreground emission, it is more likely to be real cosmic variance (Songaila 2004a). In assessing the significance of the opacity at $z = 6$ we need to know how the ionization rate in the IGM is evolving at lower redshifts, since the strongest signature of reionization would be an abrupt change in ionization at some redshift. In this paper, we use high signal-to-noise spectra of a large sample of quasars, including all the brightest $z > 4.5$ quasars observable from the northern hemisphere, to investigate the evolution of the transmission in the IGM from $z = 2$ to $z = 6.3$. We find that the transmission is smoothly evolving with redshift throughout the range.

2. Observations

Spectra of 25 high redshift quasars, with $4.17 < z_{\rm em} < 6.39$, were obtained for this program using ESI (Sheinis et al. 2000) on the KeckII telescope in echellette mode. The resolution was ~ 5300 for the $0.75''$ slit width used and the wavelength coverage is complete from 4000 Å to $10,000$ Å. Sample spectra and a more extensive discussion can be found in Songaila & Cowie (2002) and a complete catalog will be published in Songaila (2004b). At the red wavelengths, extremely high precision sky subtraction is required since the sky lines can be more than two orders of magnitude brighter than the quasars. In order to deal with this issue, individual half-hour exposures were made, stepped along the slit, and the median was used to provide the primary sky subtraction. Total exposure times were around 3–7 hours per quasar, and are summarized in Table 1a. The frames were then registered, filtered to remove cosmic rays and artifacts, and then added. At this point a second linear fit to the slit profile in the vicinity of the quasar was used to remove any small residual sky. The observations were made at the parallactic angle and flux calibrated using observations of white dwarf standards scattered through the night. These standards were also used to remove telluric absorption features in the spectra, including the various atmospheric bands.

The final extractions of the spectra were made using a weighting provided by the profile of the white dwarf standards. Measurements of residual flux in saturated regions of the spectra suggest that the sky subtraction leaves about 1% residuals in the faintest quasars and smaller errors in the brightest ones. We take the larger value as our systematic error. Wavelength calibrations were obtained using third-order fits to CuAr and Xe lamp observations at the begining and end of each night, and the absolute wavelength scale was then obtained by registering these wavelength solutions to the night sky lines. All wavelengths and redshifts are given in the vacuum heliocentric frame.

A low redshift comparison was provided by spectra of 25 quasars obtained for other programs. This sample is summarized in Table 1b. These spectra were taken with the HIRES spectrograph (Vogt et al. 1994) on the Keck I telescope with slit width 1.1 arcsec, giving a resolution $R = 36,000$. Details of the data reduction have been described previously (Songaila 1998).

The simplest characterization of the effects of the scattering by the forest is its averaged effect in depressing the continuum. This is usually characterized by the Oke indices (Oke & Korycansky 1982) averaged over the total Lyα, Lyβ, etc. regions of the spectrum, or by the generalization to the transmitted fraction,

$$F \equiv \left\langle \frac{f_\lambda}{f_{\rm cont}} \right\rangle \tag{1}$$

where f_λ is the observed spectrum, $f_{\rm cont}$ is the continuum level in the absence of scattering, and the brackets indicate averaging over a specified wavelength region.

Two methods have been used to compute $f_{\rm cont}$. For low resolution spectra, or for high redshift spectra for which F is very small, we can calculate $f_{\rm cont}$ only by extrapolating from emission line-free regions in the spectrum longward of the quasar's Lyα emission. Ideally one fits both the normalization and the power law index but in the highest redshift quasars there is seldom enough line-free spectrum to justify the fitting of the power law index, and

we assume instead a fixed power law index (here -1.25) and set the normalization using the region of the spectrum at a rest wavelength of 1350 Å. When F is small, as is the case at high redshifts, it is relatively insensitive to the choice of power law extrapolation. At lower redshifts, where F is close to 1, the measurement is sensitive to the extrapolation, and here it is preferable to make a local interpolation between the peaks in the spectrum to determine the continuum (Zuo & Lu 1993). This in turn depends on there being regions of low opacity where the spectrum is close to the continuum value.

We have used the continuum interpolation procedure for all of the HIRES data and for the ESI data at redshift less than $z = 4.5$, and have used the extrapolated continuum procedure for the ESI data at redshifts above 4.5. We have compared the two methods in the redshift range $4.0 < z < 4.5$ where there are still enough low opacity regions to allow us to use the continuum interpolation method but where there is substantial absorption through most of the spectrum, so that the transmission is only weakly dependent on the power law extrapolation. For the 85 measurements in this range in the ESI spectra, we find that, for a power law extrapolation with index 1.25, the ratio of the measured value relative to the interpolated continuum transmission is 0.84 with a dispersion of ± 0.18. For an extrapolation with a power law index of 1.75, this becomes 0.92 ± 0.20. The measured transmission fractions lie in the range 0.2 to 0.6 so this is a relatively small correction and the slightly lower value of the continuum interpolation method is caused in part by its tendency to over-estimate the transmission slightly because the continuum fitting regions have some opacity themselves. This effect becomes larger with increasing redshift. However, because the local continuum fitting method is more robust for individual quasars, we have chosen to use it for the ESI data below $z = 4.5$ and it is these values that are quoted in Table 2.

Fluxes were measured in regions of the spectrum away from the emission lines, namely: for Lyα, in 8 bins of width 15 Å between 1080 Å and 1185 Å; for Lyβ, in two 15 Å bins from

980 Å to 1010 Å; for Lyγ, in 1 bin of width 15 Å from 955 Å to 970 Å. The mean transmitted fractions for Lyα and Lyβ are plotted in Figs. 1a and 1b (small filled squares) as a function of redshift for the $z > 4.5$ ESI sample. Large open squares indicate quasars with BALQSO signatures, but the transmission of these objects do not appear to differ significantly at these wavelengths and we do not subequently distinguish these. The transmissions as a function of redshift are summarized in Table 2. The transmitted fluxes blueward of Lyα and Lyβ in the HIRES sample, measured in the same rest-frame redshift bins as for the ESI sample, are plotted as crosses in Figures 1a and 1b and tabulated in Table 2. Diamonds denote the ESI measurements with $4 < z < 4.5$, made with the local interpolation method. Values of the transmitted flux in the redshift range $z < 5$ are in general agreement with the observations of Schneider, Schmidt & Gunn (1991) and Kennefick, Dgorgovski & de Carvalho (1995) and with the earlier literature quoted in these papers. See also Songaila & Cowie (2002) for a comparison. At redshifts $z > 5$, they are also in general agreement with the results of White et al (2003). The Lyα optical depths from White et al. are shown in Fig. 2a for the quasars SDSS 1148+5251 (open diamonds) and SDSS 1030+0524 (open squares).

For purposes of display, it is useful to define a quantity $\tau_{\rm MEAN} = -\log$(transmitted fraction)but it is important to remember that this is *not* the average of the optical depth. In particular, $\tau_{\rm MEAN}$ for Lyβ is not simply related to $\tau_{\rm MEAN}$ for Lyα but is a complex function of the structure (Fan et al. 2002; Songaila & Cowie 2002). Incorrect interpretation of this quantity as a simple optical depth, as has been done in Becker et al. (2002) and White et al. (2003), results in large overestimates of the Lyα optical depth constraints based on Lyβ transmission. Using the mean of the Lyα and Lyβ transmissions, averaged in six-point bins, we have computed the corresponding Lyα and Lyβ $\tau_{\rm MEAN}$ as a function of the median redshift of each bin. These are shown in Figures 2a and 2b, where the error bars show the range of optical depths corresponding to the maximum and minimum values of transmitted flux in each bin.

3. Discussion

A uniform ionized IGM would have a Lyα optical depth

$$\tau_u = 14\,\Gamma_{-12}^{-1}\,T_4^{-0.75}\left(\frac{\Omega_m}{0.35}\right)^{-0.5}\left(\frac{\Omega_b h^2}{0.0325}\right)^{2}\left(\frac{H_0}{65\ \mathrm{km\ s^{-1}\ Mpc^{-1}}}\right)^{-1}\left(\frac{1+z}{7}\right)^{4.5} \equiv 14 g^{-1}\left(\frac{1+z}{7}\right)^{4.5} \quad (2)$$

where Γ_{-12} is the local ionization rate produced by the metagalactic ionizing flux in units of 10^{-12} s^{-1}, T_4 is the gas temperature in units of 10^4 K, and the second part of the equation defines g, which is the normalized ionization rate. For such a medium, τ_β is simply $= 0.16\tau_\alpha$, where the numerical factor is the ratio of $(f\lambda)$ for the two lines, where f is the oscillator strength. (Note that Becker et al. (2002), Fan et al. (2002) and White et al. (2003) incorrectly used only the ratio of the oscillator strengths.) The dashed lines in Figs. 2a and 2b show this shape for a constant Γ and T_4 (or constant g), where we have chosen the normalization to provide a rough match to the Lyα lines. This greatly oversimplified model gives a surprisingly good representation of the Lyα transmission over the full redshift range but underpredicts Lyβ, as can be seen in Figure 2b.

At $z \sim 4.5$ the average-density IGM begins to have substantial optical depth and it is at this point that very few regions return close to the extrapolated power law continuum as even the underdense regions have some significant opacity. It is also at this point that the transmission starts to fall extremely rapidly as the underdense voids themselves become opaque and there are no longer any regions of the IGM that transmit significantly. In this limit, it is clear why the ionized Gunn-Peterson formula is a relatively good approximation, since the bulk of the volume of the IGM is opaque and also relatively slowly evolving in filling factor and density. Because the transmission at high redshifts is dominated by the lowest density "voids" corresponding to the most underdense regions that occupy a significant volume, and since these regions evolve in a very slow and straightforward way, it is possible to characterize very simply the evolution of the mean transmission. Songaila & Cowie (2002)

derived the formula

$$F(z,g) = 4.5\, g^{-0.28} \left(\frac{1+z}{7}\right)^{2.2} \exp\left(-4.4\, g^{-0.4} \left(\frac{1+z}{7}\right)^{3}\right) \tag{3}$$

for the mean Lyα transmission as a function of redshift for the ΛCDM model of Cen & McDonald. This analytic result closely matches the exact calulations of of McDonald and collaborators (McDonald & Miralda-Escudè 2001, Cen & McDonald, 2002). It can be generalized to calculate the transmission at Lyβ:

$$F_\beta(z,g) = F(g, z_\beta)\, F(g/0.16, z) \tag{4}$$

which is simply the product of the Lyβ transmission and Lyα transmission at the redshift $1+z_\beta \equiv (\lambda_\beta/\lambda_\alpha)(1+z)$. Since we do not expect any substantial dependence on cosmology for any model that matches the lower redshift Lyα forest, these equations allow us to express the evolution of the transmission in terms of the redshift evolution of the ionization parameter, g. For Lyα, we use Equation (1) to fit the transmitted flux, assuming g is a power law function of $(1+z)$, and obtain $g = 0.74 \times ((1+z)/6)^{-4.1}$. Following the prescription given above, the Lyβ transmission is then determined and is given by equations (3) and (4). For this more realistic model, the ratio of the Lyβ and Ly α transmissions is 0.4, which is a factor of 2.5 times larger than the value of 0.16 which is valid for the ionized Gunn-Peterson case. As a consequence, models that fit Lyα, such as the simple power law ionization we have assumed here, also provide a reasonable fit to Lyβ, as can be seen in Figs. 2a and 2b.

However, rather than fitting simple models for the ionization, it is better to simply invert the equation (McDonald et al. (2000)), and in Figure 3 we have shown the ionization parameter at each redshift which would be required to produce the observed mean transmission. Using Equation (3), we have calculated the ionization rate corresponding to the mean Lyα transmissions computed in 12-point bins, starting with the highest redshift. These are displayed as the small filled squares in Figure 3. The horizontal error bars show the range of

redshift in each bin and the vertical error bars show the ionization parameter corresponding to ± 1 σ in the mean transmission in each bin. The open squares are the measurements of McDonald et al. (2000) at lower redshift. The dashed line is the power law fit to the presently measured values of g for $z > 4$ given above. The simple formula of Equation (2) is valid only at $z > 4$, so we show the interpretation of the data only above that point. As long as Ly α transmission is detectable, the Ly α measurement should give the most sensitive and reliable measurement of g. However where Lyα is not seen, the Lyβ can give a more sensitive constraint because of its weaker oscillator strength (Becker et al. 2002; Fan et al. 2002; White et al. 2003). We note that there is some sign in Fig. 2b that the Lyβ opacity may be high relative to Lyα in the highest redshift bin. The value of g would be 0.03 at $z = 6.05$ if we used Lyβ, which is more consistent with Fan et al. (2002) though it still lies above their upper limit. However, we emphasise that the Lyα values are more robust. This drop off in the ionization parameter must also be combined with the mean free path for ionizing photons to determine the actual production rate of ionizing photons. This in turn means that the fall off in the rate of ionizing photon production is shallower than the fall-off in g. We postpone a more detailed discussion of this to a subsequent paper.

4. High Redshift Colors

Precise measurements of the forest transmission are also invaluable for determining the colors of high redshift galaxies and quasars. Currently the effects are usually included using the Madau (1995) models which are based on early data in the range $2 < z < 5$. The present data can be used instead to compute these colors on an empirical basis and also to compute how much change can be produced by cosmic variance in the forest scattering. For broad band filters this latter effect is very small at all redshifts but it can be significant if narrow band filters are used.

As a useful example, we have computed the expected magnitude change as a function of redshift for the case of a flat f_ν spectrum galaxy with a complete break at the Lyman continuum edge, which should be representative of typical high redshift galaxies. For each of 5 colors (Johnson B and V, Kron-Cousins R and I and Sloan z) we computed the convolution of the spectrum with the filter transmission and the forest transmission and computed the decrement relative to a flat f_ν object without a break. For regions of the spectrum where the Lyα forest would lie in the filter we interpolated the numbers in Table 2a to determine the average transmission, and similarly for the Lyβ transmission from Table 2b. For wavelengths between the Lyman continuum break and the Lyγ line we used the results of Table 2c. The results are relatively insensitive to this approximation of the higher order Lyman series scattering. The results are shown in Figure 4 and summarised in Table 3 where the changes in magnitudes produced by the decrement are given. The difference between the magnitude shifts in any two filters gives the color of the galaxy at the redshift in the AB magnitude system of Oke. Therefore, at $z = 5.7$, for example, the AB $(R - z)$ color is 2.19. Similar results may be computed for any input spectrum using the transmissions in the tables.

5. Conclusions

We have measured the transmission of the Lyα forest produced by neutral hydrogen scattering in the intergalactic medium between redshifts 2 and 6.3 using high signal to noise, high resolution ($R \geq 5000$) observations of 50 quasars spread over the redshift range. The transmitted fractions show a relatively smooth evolution over the entire range of redshifts, which can be modelled with a smoothly decreasing ionization rate. We have used the tabulated transmissions to calculate the colors of a flat-spectrum galaxy with a large intrinsic Lyman continuum break.

I would like to thank X. Fan and R. Becker for providing the coordinates of some of the $z > 6$ quasars prior to their publication and for useful comments on the first draft, and Michael Strauss and Robert Lupton for helpful dicsussions. Peter Shaver kindly provided a critical reading of the first draft. This research was supported by the National Science Foundation under grant AST 00-98480.

REFERENCES

Becker, R. H., et al. 2002, AJ, 122, 2850.

Bennett, C. L., Halpern, M., Hinshaw, G., et al. 2003, ApJS, 148, 1.

Cen, R. & McDonald, P. 2002, ApJ, 570, 457.

Djorgovski, S. G., Castro, S. M., Stern, D. & Mahabel, A. A. 2001, ApJ, 560, L5.

Fan, X. et al. 2002, AJ, 123, 1247.

Fan, X. et al. 2003, AJ, 125, 1649.

Gnedin, N. Y. 2002,

Kennefick, J. D., Djorgovski, G. & De Carvalho, R. R. 1995, AJ, 110, 2553.

Oke, J. B. & Korycansky, D. G. 1982, ApJ, 255, 11.

Madau, P. 1995, ApJ, 441, 18.

McDonald, P. & Miralda-Escudé, J. 2001, ApJ, 549, L11.

McDonald, P., Miralda-Escudè, J., Rauch, M., Sargent, W. L. W. et al. 2000, ApJ, 543, 1.

Schneider, D. P., Schmidt, M. & Gunn, J E. 1991, AJ, 101, 2004.

Sheinis, A. I., Miller, J. S., Bolte, M. & Sutin, B. M. 2000, Proc. SPIE, 4008, 522.

Songaila, A. 1998, AJ 115, 2184.

Songaila, A. & Cowie, L. L. 2002, AJ, 123, 2183.

Songaila, A. 2004a, in preparation.

Songaila, A. 2004b, in preparation.

Vogt, S. S., et al. 1994, S.P.I.E., 2198, 362.

White, R. L., Becker, R. H., Fan, X., & Strauss, M. A. 2003, AJ, 126, 1.

Zuo, L. & Lu, L. 1993, ApJ, 418, 601.

This manuscript was prepared with the AAS LaTeX macros v4.0.

Table 1a. High Redshift ESI Observations

Quasar	Mag.	Expo. (hrs)	z_{em}
SDSS 0206+1216	19.9	3.0	4.81
SDSS 0211−0009	20.0	7.0	4.90
SDSS 0231−0728	19.2	4.33	5.42
SDSS 0338+0021	20.0	7.25	5.01
BR 0353−3820	18.0	2.5	4.58
PSS 0747+4434	18.1	3.0	4.39?
FIRST 0747+2739	17.2	1.5	4.17
SDSS 0756+4104	20.1	3.0	5.09
SDSS 0836+0054	18.8	6.0	5.82
BRI 0952−0115	18.7	4.25	4.42
SDSS 1030+0524	19.7	6.28	6.28
BR 1033−0327	18.5	2.0	4.51
SDSS 1044−0125	19.7	5.75	5.74
SDSS 1048+4637	18.4	6.23	6.23
SDSS 1148+5251	19.1	6.39	6.39
SDSS 1204−0021	19.1	3.0	5.07
BR 1202−0725	18.7	3.0	4.61
SDSS 1306+0356	19.6	6.75	5.99

Table 1a—Continued

Quasar	Mag.	Expo. (hrs)	z_{em}
SDSS 1321+0038	20.1	2.0	4.71
SDSS 1605−0122	19.4	3.75	4.93
WFSJ 1612+5255	19.9	1.5	4.95
SDSS 1737+5828	19.3	7.5	4.85
SDSS 2200+0017	19.1	5.3	4.78
SDSS 2216+0013	20.3	3.0	5.00
BR 2237−0607	18.3	11.6	4.55

Table 1b. Low Redshift HIRES Observations

Quasar	Mag.	Expo. (hrs)	z_{em}
Q0014+813	16.5	7.8	3.38
HS0119+1432	16.7	7.8	2.87
Q0256-000	18.7	5.5	3.37
Q0302-003	18.4	10.7	3.28
Q0636+680	16.5	7.4	3.18
HS0741+4741	17.5	8.0	3.22
HS0757+5218	17.5	4.0	3.2
Q08279+5255	15.2	3.8	3.87
Q0956+122	18.2	7.3	3.30
Q1032+0414	18.1	4.0	3.39
J1057+4555	17.7	11.3	4.10
HE1104-1805	16.3	2.0	2.31
HE1122-1648	16.6	3.5	2.40
Q1159+123	17.5	8.0	3.50
Q1206+119	17.9	5.0	3.113
B1310+4254	18.4	5.2	2.561
Q1422+2309	16.7	16.2	3.63
Q1623+269	16.0	4.0	2.52

Table 1b—Continued

Quasar	Mag.	Expo. (hrs)	z_{em}
FBQS1634+3203	16.6	4.0	2.35
HS1700+6416	16.1	11.0	2.748
Q1937-1009	17.5	9.3	3.805
HS1946+7658	15.8	12.0	3.02
Q2000-330	17.6	4.7	3.77
Q2126-158	17.3	4.4	3.28
HE2347-4342	16.1	6.7	2.88

Table 2a. Mean Transmission Blueward of Lyα

$z_{\rm median}$	$\langle T \rangle$	$T_{\rm max}$	$T_{\rm min}$
2.40	0.820	0.900	0.710
2.46	0.809	0.879	0.735
2.54	0.818	0.899	0.761
2.61	0.778	0.833	0.700
2.67	0.728	0.839	0.608
2.72	0.800	0.893	0.702
2.75	0.780	0.837	0.700
2.79	0.764	0.811	0.648
2.83	0.698	0.806	0.575
2.86	0.695	0.806	0.552
2.89	0.729	0.808	0.643
2.92	0.694	0.799	0.492
2.95	0.788	0.847	0.744
2.98	0.712	0.812	0.644
3.01	0.723	0.833	0.618
3.03	0.692	0.821	0.456
3.08	0.697	0.774	0.639
3.09	0.719	0.855	0.545

Table 2a—Continued

$z_{\rm median}$	$\langle T \rangle$	$T_{\rm max}$	$T_{\rm min}$
3.14	0.767	0.849	0.711
3.19	0.717	0.785	0.650
3.24	0.675	0.713	0.630
3.35	0.687	0.800	0.597
3.48	0.628	0.730	0.532
3.59	0.597	0.729	0.467
3.65	0.553	0.633	0.449
3.75	0.495	0.574	0.414
3.84	0.495	0.624	0.352
3.89	0.563	0.803	0.290
3.94	0.487	0.612	0.363
3.99	0.467	0.565	0.346
4.03	0.388	0.469	0.302
4.08	0.434	0.577	0.297
4.12	0.491	0.640	0.367
4.17	0.487	0.554	0.419
4.20	0.441	0.577	0.342
4.23	0.414	0.492	0.348

Table 2a—Continued

$z_{\rm median}$	$\langle T \rangle$	$T_{\rm max}$	$T_{\rm min}$
4.26	0.404	0.487	0.309
4.29	0.300	0.453	0.135
4.31	0.439	0.588	0.326
4.35	0.350	0.420	0.279
4.37	0.398	0.551	0.219
4.41	0.426	0.621	0.288
4.44	0.348	0.397	0.253
4.48	0.328	0.401	0.277
4.52	0.316	0.408	0.187
4.56	0.376	0.472	0.247
4.59	0.297	0.366	0.148
4.66	0.222	0.317	0.110
4.68	0.215	0.273	0.093
4.74	0.238	0.303	0.194
4.82	0.246	0.334	0.200
4.98	0.182	0.222	0.151
5.13	0.147	0.321	0.095
5.26	0.084	0.208	0.016

Table 2a—Continued

$z_{\rm median}$	$\langle T \rangle$	$T_{\rm max}$	$T_{\rm min}$
5.42	0.090	0.150	0.027
5.51	0.060	0.161	0.025
5.60	0.082	0.178	0.044
5.70	0.028	0.071	-0.001
5.87	0.009	0.025	-0.001
6.05	0.0006	0.007	-0.002

Table 2b. Mean Transmission Blueward of Lyβ

$z_{\rm median}$	$\langle T \rangle$	$T_{\rm max}$	$T_{\rm min}$
3.06	0.735	0.820	0.627
3.18	0.718	0.785	0.624
3.27	0.707	0.801	0.616
3.52	0.641	0.700	0.585
4.05	0.502	0.611	0.394
4.30	0.502	0.582	0.433
4.42	0.457	0.560	0.380
4.59	0.378	0.625	0.200
4.71	0.253	0.413	-0.013
4.81	0.243	0.328	0.085
4.95	0.258	0.353	0.162
5.66	0.082	0.140	0.035
6.11	0.0002	0.009	-0.008

Table 2c. Mean Transmission Blueward of Lyγ

$z_{\rm median}$	$\langle T \rangle$	$T_{\rm max}$	$T_{\rm min}$
3.32	0.715	0.749	0.650
4.04	0.428	0.668	-0.422
4.49	0.449	0.541	0.373
4.78	0.249	0.549	-0.039
5.00	0.240	0.416	0.173
6.15	0.038	0.126	-0.001

Table 3. Colors of High redshift Galaxies and Quasars

Redshift	z	I	R	V	B
3.0	0.00	0.00	0.00	0.00	0.37
3.1	0.00	0.00	0.00	0.01	0.48
3.2	0.00	0.00	0.00	0.04	0.59
3.3	0.00	0.00	0.00	0.08	0.65
3.4	0.00	0.00	0.00	0.13	0.68
3.5	0.00	0.00	0.00	0.18	0.72
3.6	0.00	0.00	0.00	0.25	0.84
3.7	0.00	0.00	1.10	0.33	1.00
3.8	0.00	0.00	0.00	0.43	1.17
3.9	0.00	0.00	0.02	0.51	1.41
4.0	0.00	0.00	0.07	0.56	1.76
4.1	0.00	0.00	0.14	0.60	2.17
4.2	0.00	0.00	0.21	0.65	2.68
4.3	0.00	0.00	0.29	0.69	3.55
4.4	0.00	0.00	0.39	0.72	5.39
4.5	0.00	0.00	0.50	0.85	7.80
4.6	0.00	0.00	0.62	1.01	9.19
4.7	0.00	0.00	0.79	1.29	10.5

Table 3—Continued

Redshift	z	I	R	V	B
4.8	0.00	0.00	0.99	1.63	12.2
4.9	0.00	0.00	1.13	1.97	13.6
5.0	0.00	0.03	1.19	2.30	18.2
5.1	0.00	0.10	1.24	2.56	25.0
5.2	0.00	0.18	1.30	2.92	25.0
5.3	0.00	0.29	1.39	3.42	25.0
5.4	0.00	0.42	1.51	4.06	25.0
5.5	0.00	0.56	1.69	5.31	25.0
5.6	0.00	0.72	1.94	6.98	25.0
5.7	0.00	0.91	2.19	8.71	25.0
5.8	0.00	1.16	2.52	10.0	25.0
5.9	0.01	1.46	2.97	11.1	25.0
6.0	0.04	1.87	3.38	12.3	25.0
6.1	0.12	2.57	3.83	14.0	25.0
6.2	0.23	3.30	4.34	20.4	25.0
6.3	0.35	3.66	4.83	25.0	25.0
6.4	0.49	3.93	5.45	25.0	25.0

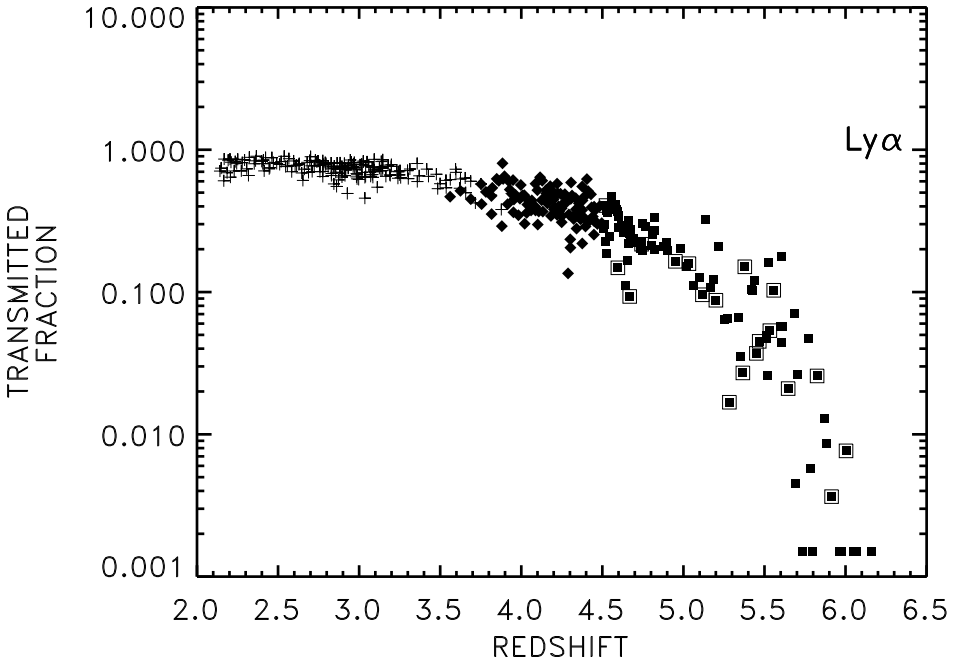

Fig. 1a.— Transmitted flux blueward of Lyα emission as a function of redshift for both the ESI and HIRES samples. In all cases, flux was computed in 8 bins of width 15 Å between 1080 Å and 1185 Å. For the $z > 4.5$ ESI sample (filled squares), the flux was normalized to a quasar power law continuum with slope -1.25 normalized at 1350 Å. Large open squares denote data for real or suspected BAL QSOs in the sample, namely SDSS 1605−0112, SDSS 1044−0125, and SDSS 1048+4637. For the lower redshift HIRES sample (crosses), the flux was normalized to a continuum that was interpolated locally between transmission peaks. For the $z < 4.5$ ESI sample, the continuum was computed by both methods and is plotted (diamonds) assuming the local interpolation. See text for a discussion of the comparison. Where the transmitted flux is less than 0.0015, we have shown it at this nominal value.

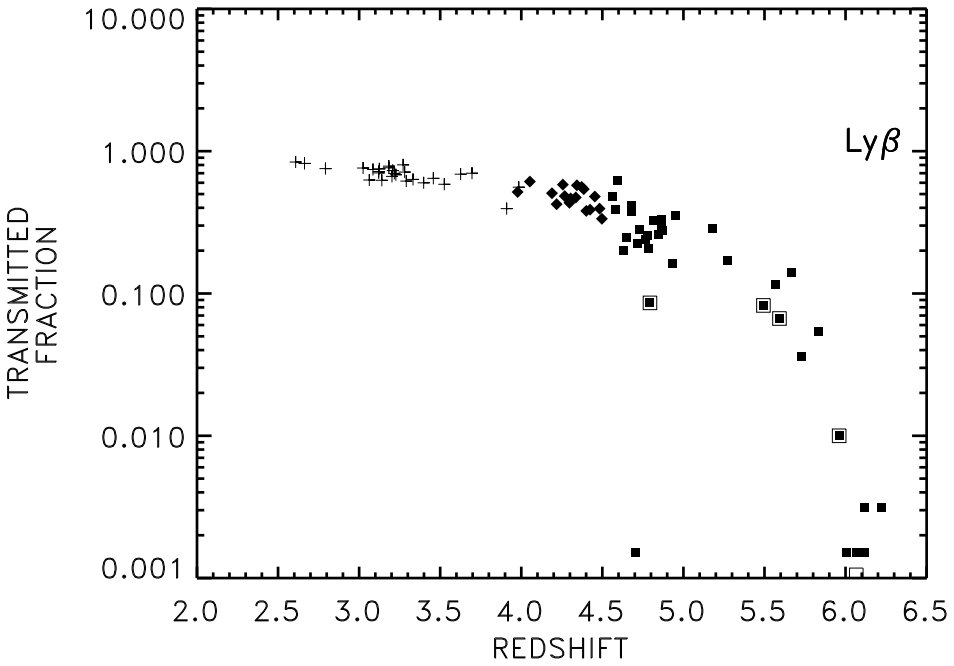

Fig. 1b.— As in Fig. 1a for transmission blueward of Lyβ. Flux was computed in two bins of width 15Å between 980Å and 1010Å.

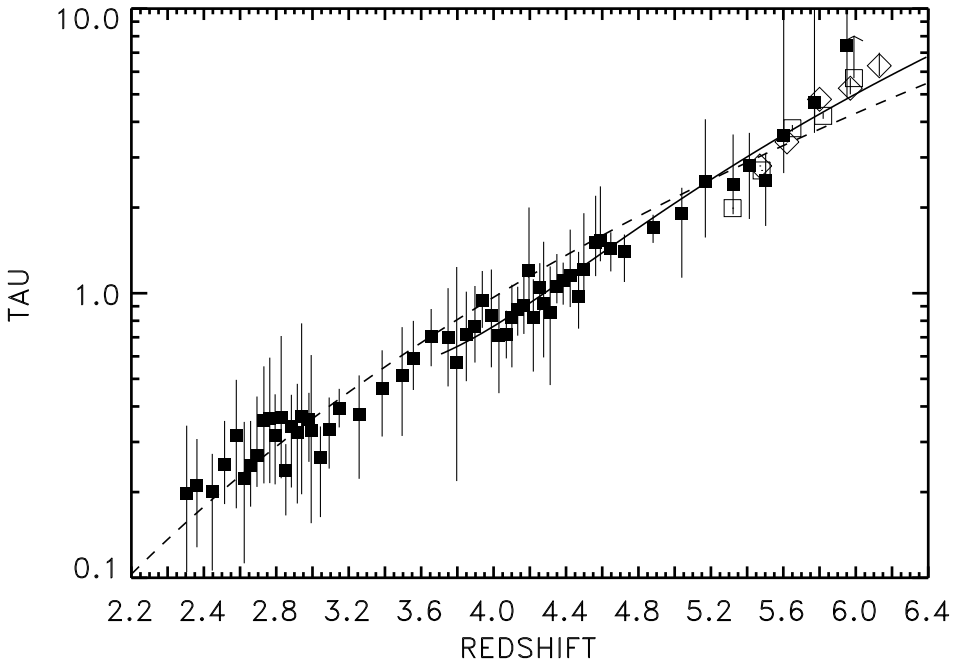

Fig. 2a.— Optical depth blueward of Lyα emission as a function of redshift for the complete sample of Figure 1a. Starting with the highest redshift points, mean transmissions were computed in bins of six data points. The optical depths corresponding to the mean transmissions are plotted (filled squares) as a function of the median redshift in each bin. The error bars show the range of extremes of transmission within each bin, converted to optical depth. Mean transmissions and median redshifts in each bin are tabulated in Table 2a, along with the redshift range in each bin. The dashed line shows a uniform ionized Gunn-Peterson model, normalized to match the observations. The solid line is the model of Equation (2), with g set equal to $0.74 \times ((1+z)/6)^{-4.1}$. Open symbols denote Ly$\alpha$ optical depths from Figure 6 of White et al. (2003) for the quasars SDSS 1148+5251 (diamonds) and SDSS 1030+0524 (squares).

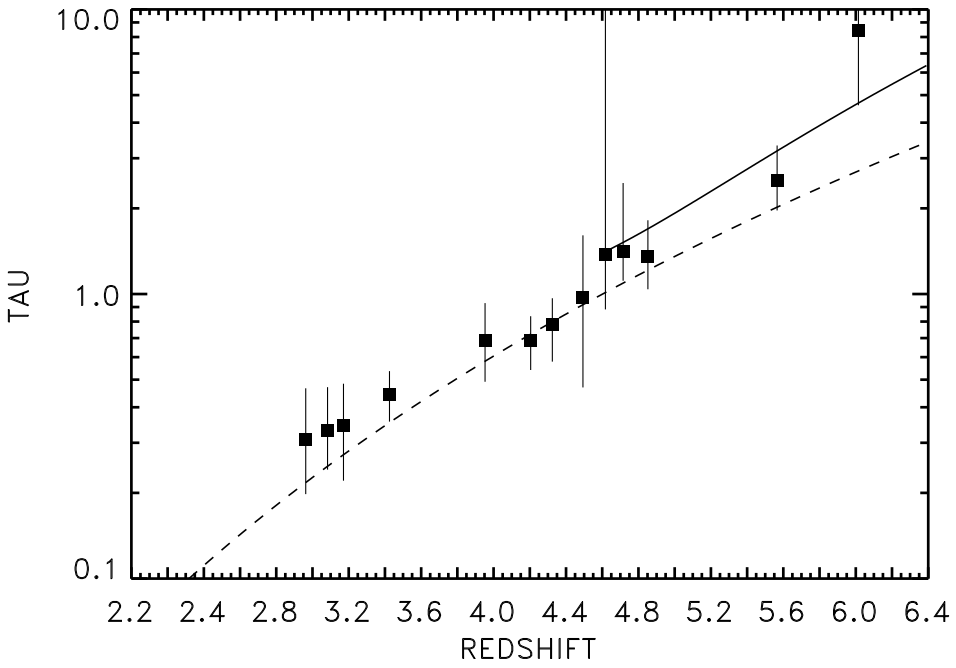

Fig. 2b.— As in Fig. aA for Ly β. The dashed line is a uniform ionized Gunn Peterson model for Ly β, computed with the same normalization as in Figure 2a. It underpredicts the Ly β absorption because of the inhomogeneous nature of the IGM. The solid line is the computed absorption from Equation 3 for the same run of ionization as in Figure 2a. See text for discussion.

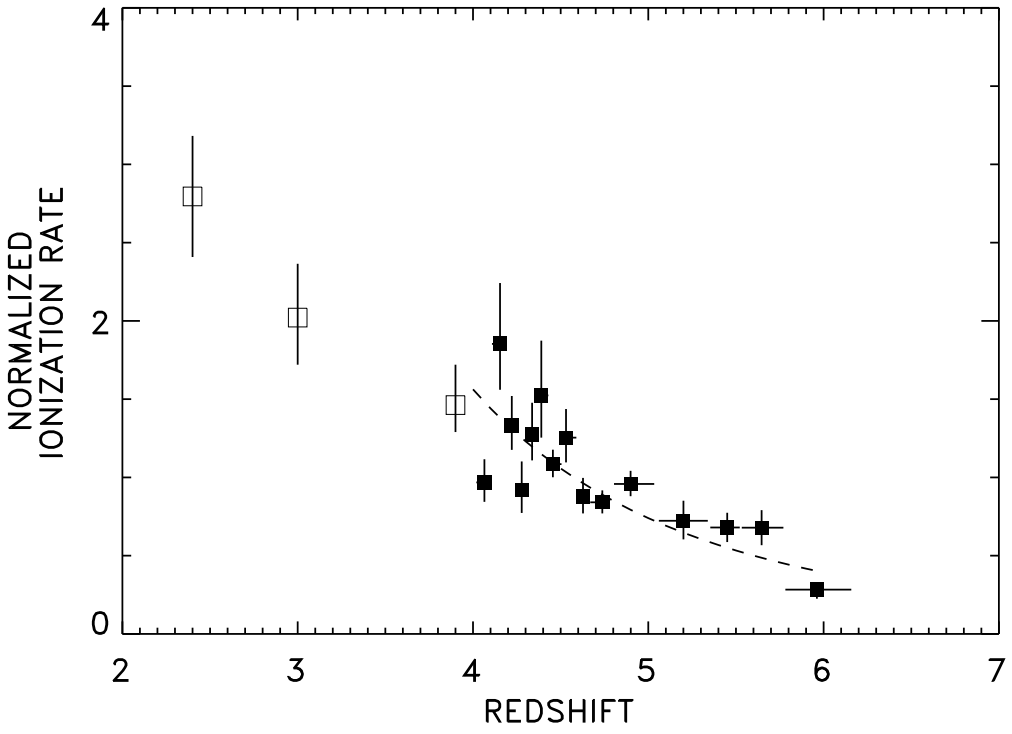

Fig. 3.— Evolution of the normalized ionization rate as a function of redshift computed from mean transmissions using Equation 2 (*filled squares*). Mean transmissions and dispersions and median redshifts were computed in 12-point bins, starting at the highest redshift. The horizontal error bars show the range of redshift in each bin and the vertical error bars show the ionization parameter corresponding to ± 1 σ in the mean transmission in each bin. The open squares are the measurements of McDonald et al. (2000) at lower redshift. The dashed line is a power law of the form $0.74 \times ((1+z)/6)^{-4.1}$, fitted to the present data for $z > 4$.

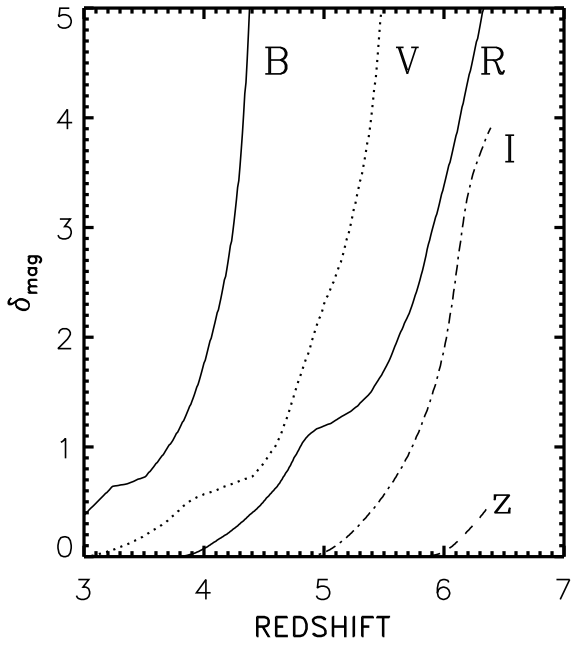

Fig. 4.— Magnitude change expected as a result of IGM opacity as a function of redshift for a flat f_ν spectrum galaxy with a complete break at the Lyman continuum edge, for each of 5 colors: Johnson B and V, Kron-Cousins R and I and Sloan z. The Suprime-Cam filter transmissions (http://www.noaj.org/Observing/Instruments/SCam/sensitivity.html) were used for the specific transmissions adopted. Approximate forest decrements were computed from the Lyα, Lyβ, and Lyγ transmissions of Table 2.